Available online at www.sciencedirect.com
SCIENCE DIRECT®
Journal of Sound and Vibration 273 (2004) 949–968
JOURNAL OF SOUND AND VIBRATION
www.elsevier.com/locate/jsvi

Stability and chaotic dynamics of a rate gyro with feedback control under uncertain vehicle spin and acceleration

Heng-Hui Chen*

Department of Mechanical Engineering, HsiuPing Institute of Technology, Gungye Road 11, Taichung 412, Taiwan, ROC

Received 4 October 2002; accepted 6 May 2003

Abstract

An analysis of stability and chaotic dynamics is presented by a single-axis rate gyro subjected to linear feedback control loops. This rate gyro is supposed to be mounted on a space vehicle which undergoes an uncertain angular velocity $\omega_Z(t)$ around its spin axis. And simultaneously acceleration $\dot{\omega}_X(t)$ occurs with respect to the output axis. The necessary and sufficient conditions of stability for the autonomous case, whose vehicle undergoes a steady rotation, were provided by Routh–Hurwitz theory. Also, the degeneracy conditions of the non-hyperbolic point were derived and the dynamics of the resulting system on the center manifold near the double-zero degenerate point by using center manifold and normal form methods were examined. The stability of the non-linear non-autonomous system was investigated by Liapunov stability and instability theorems. As the electrical time constant is much smaller than the mechanical time constant, the singularly perturbed system can be obtained by the singular perturbation theory. The Liapunov stability of this system by studying the reduced and boundary-layer systems was also analyzed. Numerical simulations were performed to verify the analytical results. The stable regions of the autonomous system were obtained in parametric diagrams. For the non-autonomous case in which $\omega_Z(t)$ oscillates near boundary of stability, periodic, quasiperiodic and chaotic motions were demonstrated by using time history, phase plane and Poincaré maps.

1. Introduction

The field of applications of gyroscope is widespread, such as in the navigation and control system, due to its distinctive property. Here, a single-axis rate gyro is used for the measurement of angular velocity in spinning space vehicles. For all applications, it is a critical problem to show the stability of motion of the gyro, both theoretically and practically.

*Fax: +8864-24961187.
E-mail address: richard@mail.hit.edu.tw (H.-H. Chen).

0022-460X/03/$ - see front matter © 2003 Elsevier Ltd. All rights reserved.
doi:10.1016/S0022-460X(03)00510-8

Several interesting problems had been studied previously in the analysis of motion of the gimbals of rate gyros in spinning vehicles [1–4]. For the case of which ω_Z is an uncertain constant, conditions for global and local asymptotic stability of the gyro in spinning vehicles had been obtained by using the Liapunov approach [1]. Under considerations of an angular velocity of vehicle about its spin axis and an angular acceleration of the vehicle about its output axis the motion of a single-axis rate gyro had been examined for small rotation θ of the gimbals [2,3]. The stability of a rate gyro mounted on a vehicle, which has a time-varying angular velocity about its spin axis, was studied by the Liapunov direct method [4]. All of the above references are two-dimensional systems. An analysis of stability, double degeneracy and chaotic dynamics is presented by a rate gyro with feedback control mounted on a space vehicle that spins with an uncertain angular velocity $\omega_Z(t)$ around its spin axis [5,6]. This system is a three-dimensional non-linear one.

When it is referred to chaos in some parametric space, a non-linear system can also exhibit complicated steady state behaviors [7]. After numerical analysis of meteorology, Lorenz discovered the chaotic attractor, which is so-called "deterministic chaos". There will be a sensitive dependence on initial conditions of time histories of chaotic motion, when some non-linearities exist in system [7–11]. There are many routes to chaos in dissipative systems. Three prominent routes to chaos have been explored. They are period doubling, intermittency, and quasiperiodic routes. And the three routes can be related to period doubling, saddle node, and Hopf bifurcations respectively [7–9]. In gyroscopic systems, the dynamics of gyros also exhibit chaotic behavior. In this paper, the parametrically excited system is studied. It will exhibit non-linear phenomena including the existence of periodic, quasiperiodic and chaotic motions of the system.

Singular perturbations, traditional efficient tools for determining physically meaningful subsystems, are being developed into systematic approach to multi-time dynamic systems. These methods applied in power systems and Markov chains were used to decompose the dynamic systems into reduced (slow) and boundary-layer (fast) systems [12,13]. Cited from those methods, the singular perturbation method is also used to derive the special form of the gyro system.

In this paper, the stability and chaotic dynamics of a single-axis rate gyro subjected to linear feedback control mounted on a space vehicle undergoing uncertain angular velocity $\omega_Z(t)$ about its spin of the gyro and acceleration $\dot{\omega}_X(t)$ with respect to the output axis are studied. The controller of the system is modelled by the first order dynamics with a time constant of $O(1)$ so that the feedback control system is a three-dimensional one. For the case of which ω_Z is an uncertain constant, the stability conditions and bifurcation surfaces of the system were derived by Routh–Hurwitz theory and local bifurcation analysis to reveal region of stability and bifurcation sequences with the associated phase portraits in the parametric space, in the neighborhood of the double degeneracy. For the non-linear non-autonomous system, the stability of the feedback control system will be obtained by using the Liapunov direct method. When the time constant of controller is much smaller than the mechanical one, the singularly perturbed system can be obtained by singular perturbation theory. Studying the reduced and boundary-layer systems also analyze the Liapunov stability of this system. Finally, the degeneracy conditions of the system are presented in parametric planes by numerical simulations. The numerical results of the perturbation of an uncertain angular velocity undergoing small harmonic excitation are carried out to examine the various forms of dynamic behavior by using the time history, phase plane, Poincaré maps.

2. Equations of motion

We considered the model of a single-rate gyro mounted on a space vehicle as shown in Fig. 1. The gimbals can turn about output X-axis with rotational angle θ. Damping torque $C_d\dot{\theta}$ resists motion about this axis. Using Lagrange's equation, the differential equation for the output deflection angle θ of a rate gyro with feedback control was derived as follows [14]:

$$(A + A_g)\ddot{\theta} + C_d\dot{\theta} + Cn_R(\omega_Y \cos\theta + \omega_Z \sin\theta) + (A + B_g - C_g)(\omega_Y \cos\theta + \omega_Z \sin\theta)(\omega_Y \sin\theta - \omega_Z \cos\theta) + (A + A_g)\dot{\omega}_X = T_c, \tag{1}$$

where $Cn_R = C(\dot{\psi} - \omega_Y \sin\theta + \omega_Z \cos\theta) = const.$

ω_X, ω_Y, and ω_Z denote the angular velocity components of the platform along output axis X, input axis Y, and normal axis Z respectively. A, A $(= B)$, C and A_g, B_g, C_g denote the moments of inertia of rotor and gimbals for the gimbals axes ξ, η, ζ respectively. T_c is the control-motor torque along the output axis of the system to balance the corresponding gyroscopic torque. The torque and electric current of control-motor can be modelled by the following relationships:

$$T_c = K_T I, \tag{2}$$

$$L\dot{I} + RI = K_a(\theta_d - \theta) - K_0\dot{\theta}, \tag{3}$$

where electromotive force is proportional to the difference between the prescribed motion $\theta_d(t)$ and the rotational angle θ, that is $u = K_a(\theta_d - \theta)$. It is applied to the control-motor. I, R, L, and K_0 are the current, resistance, inductance, and back-electromotive constant of the control-motor; K_T denotes the torque constant of the control-motor.

Eqs. (1)–(3) thus represent a feedback control system when position feedback is applied to the gyro motion. The prescribed motion of the gyro needs to be fixed at the origin, i.e. $\theta_d = 0$, where the relationship of the output angle θ is proportional to the constant input angular velocity ω_Y. It is very important to analyze the stability of the measuring origin of a rate gyro system mounted on

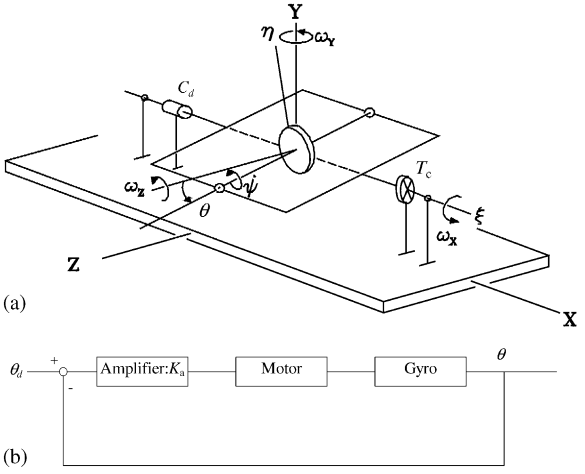

Fig. 1. The feedback system: (a) the rate gyro; (b) the block diagram.

a wobbling space vehicle, because the more precise analysis for the system, the more reliability for the guidance.

We are interested in the non-linear behavior of dynamical motion when the vehicle undergoes an uncertain angular velocity $\omega_Z(t)$ about the spin axis (Z-axis), an acceleration $\dot{\omega}_X(t)$ about the output axis (X-axis), and the angular velocity about OY is zero, i.e., $\omega_Y = 0$. Now the feedback control system is studied in the following form:

$$\begin{aligned} \dot{x} &= y, \\ \dot{y} &= -D_1 y + D_2 z - D_3 \omega_Z(t) \sin x + 1/2 D_4 \omega_Z^2(t) \sin 2x - \dot{\omega}_X, \\ \dot{z} &= -D_5 z - D_6 x - D_7 y, \end{aligned} \tag{4}$$

where $x = \theta, y = \dot{\theta}, z = I, D_1 = C_d/(A + A_g)$, $D_2 = K_T/(A + A_g)$, $D_3 = Cn_R/(A + A_g)$, $D_4 = (A + B_g - C_g)/(A + A_g)$, $D_5 = R/L, D_6 = K_a/L$, $D_7 = K_0/L$.

3. The stability of gimbal motion

In this section, the stability of both autonomous system and non-autonomous system are discussed by distinct methods. The stability of the autonomous system is analyzed to obtain the necessary and sufficient conditions for locally asymptotical stable motion at the fixed point by Routh–Hurwitz criterion. In addition, the Liapunov direct method [14] was used to obtain the conditions sufficient for asymptotical stability and instability of motion of the feedback control system.

3.1. The stability of the non-linear autonomous system

For the case when $\dot{\omega}_X = 0$ and $\omega_Z = \omega_{ZC} = const.$, this system is autonomous. One stationary point of the non-linear autonomous system is the origin $(x, y, z) = (0, 0, 0)$. Let the disturbed motion be $x = 0 + x_1$, $y = 0 + x_2$, $z = 0 + x_3$, so the equations for disturbances are as

$$\begin{aligned} \dot{x}_1 &= x_2, \\ \dot{x}_2 &= -D_1 x_2 + D_2 x_3 + Q x_1 + H x_1^3 + O(x_1)^5, \\ \dot{x}_3 &= -D_5 x_3 - D_6 x_1 - D_7 x_2, \end{aligned} \tag{5}$$

where $Q = -D_3 \omega_{ZC} + D_4 \omega_{ZC}^2$, $H = D_3 \omega_{ZC}/6 - 2D_4 \omega_{ZC}^2/3$.

First, the conditions for the stability of the origin of the autonomous system will be obtained by using the Routh–Hurwitz criterion.

The Jacobian matrix $\mathbf{J}$ at the origin of system (5) is in the form of

$$\mathbf{J} = \begin{bmatrix} 0 & 1 & 0 \\ Q & -D_1 & D_2 \\ -D_6 & -D_7 & -D_5 \end{bmatrix}. \tag{6}$$

According to the Routh–Hurwitz criterion, the necessary and sufficient conditions for stability are as follows:

$$\omega_{ZC1} < \omega_{ZC} < \omega_{ZC2}, \tag{7}$$

where

$$\omega_{ZC1} = (D_3 - (D_3^2 + 4D_4 p_{min})^{1/2})/(2D_4), \quad \omega_{ZC2} = (D_3 + (D_3^2 + 4D_4 p_{min})^{1/2})/(2D_4),$$

$$p_{min} = \mathrm{Min}(e_3, e_6), \quad e_3 = (D_5 D_2 D_7 + D_1 D_5^2 + D_1 D_2 D_7 + D_1^2 D_5 - D_6 D_2)/D_1, \quad e_6 = D_6 D_2 / D_5.$$

All the roots of the characteristic polynomial of the Jacobian matrix **J** have negative real parts, i.e., the motion of the linearized autonomous system is asymptotically stable at the fixed point. Alternatively, the system possesses critical behavior when Jacobian matrix **J** contains eigenvalues with zero real parts in the following bifurcation surfaces:

1. There exists one zero eigenvalue ($\lambda_1 = 0$) of this linearized system for the system parameter $Q = D_6 D_2 / D_5$, i.e., $\omega_{ZC} = \omega_{ZC1}$ or ω_{ZC2}, on stability boundary, $p_{min} = e_6$. The residual eigenvalues are $\lambda_{2,3} = \{-(D_1 + D_5) \pm [(D_1 + D_5)^2 - 4(D_2 D_7 - Q + D_1 D_5)]^{1/2}\}/2$.
2. There exists a pair of pure imaginary eigenvalues ($\lambda_{1,2} = \pm \mathrm{j}\omega_0$) of this linearized system for the system parameter $Q = (D_5 D_2 D_7 + D_1 D_5^2 + D_1 D_2 D_7 + D_1^2 D_5 - D_6 D_2)/D_1$, i.e., $\omega_{ZC} = \omega_{ZC1}$ or $\omega_{ZC} = \omega_{ZC2}$, $p_{min} = e_3$, where $\omega_0 = (-D_1(D_5 D_2 D_7 + D_1 D_5^2 - D_6 D_2))^{1/2}/D_1$ is a real number, i.e., $D_2 > D_1 D_5^2/(D_6 - D_5 D_7)$. The residual eigenvalue is $-(D_1 + D_5)$;
3. There exists a double zero eigenvalues ($\lambda_{1,2} = 0, 0$) for (a) the system parameter $Q = D_1 D_5 D_6/(D_6 - D_5 D_7)$ and $D_2 = D_1 D_5^2/(D_6 - D_5 D_7)$, the residual eigenvalue is $-(D_1 + D_5)$; (b) the system parameter $Q = D_6 D_2 / D_5$ and $D_1 = D_2(D_6 - D_5 D_7)/D_5^2$, the residual eigenvalue is still in the form of $-(D_1 + D_5)$ but the value adapts for varying the system parameter D_1.

Here, the qualitative behaviors of this system in the neighborhood of a fixed point are examined by local bifurcation analysis. A codimension 2 bifurcation problem of the feedback system is studied. There exists a double zero eigenvalues with the third eigenvalue being $-(D_1 + D_5)$ on the surface

$$Q = Q_C = D_1 D_5 D_6/(D_6 - D_5 D_7), \quad D_2 = D_{2C} = D_1 D_5^2/(D_6 - D_5 D_7). \tag{8}$$

To transform the linear part of this system into the Jordan canonical form Λ, we use the similarity transformation matrix **T** of generalized eigenvectors of the Jacobian matrix **J**:

$$\mathbf{T} = \begin{bmatrix} 1 & a_{12} & a_{13} \\ 0 & 1 & a_{23} \\ a_{31} & 0 & 1 \end{bmatrix}, \tag{9}$$

where a_{12}, a_{13}, a_{23}, a_{23} and its determinant Δ are shown in Appendix A.

We introduce the parameters $Q = Q_C + \varepsilon_1$, $D_2 = D_{2C} + \varepsilon_2$, so that the unfolding of the critical system ($\varepsilon_1 = \varepsilon_2 = 0$) will be included in our parameterized normal form. By choosing the co-ordinate transformation $y = \mathbf{T}x$, the system equation (5) becomes the standard form

$$\dot{y} = \mathbf{\Lambda} y + \mathbf{\Lambda}_\varepsilon y + F_y, \tag{10}$$

where the non-linear function F_y is evaluated at critical values; $\mathbf{\Lambda}$, $\mathbf{\Lambda}_\varepsilon$ and F_y are shown in Appendix A. By center manifold theory [15] the study of the dynamics can be reduced to the

associated lower-dimensional center manifold to determine the key qualitative dynamical behavior. The center manifold will be computed from the standard form (10) at the critical values ($\varepsilon_1 = \varepsilon_2 = 0$). Now we will begin by considering the center manifold for this system. Eq. (5) contains cubic symmetry which implies that the center manifold will be given by an odd function $y_3 = h(y_1, y_2)$, i.e., $y_3 = O(|y_i^3|)$. Thus the corresponding reduced system is

$$\begin{bmatrix} \dot{y}_1 \\ \dot{y}_2 \end{bmatrix} = \begin{bmatrix} 0 & 1 \\ 0 & 0 \end{bmatrix} \begin{bmatrix} y_1 \\ y_2 \end{bmatrix} + \begin{bmatrix} e_{11} & e_{12} \\ e_{21} & e_{22} \end{bmatrix} \begin{bmatrix} y_1 \\ y_2 \end{bmatrix} + \begin{bmatrix} f_{yc1} \\ f_{yc2} \end{bmatrix} + \text{h.o.t.}, \tag{11}$$

then we employ a linear change of co-ordinates

$$\begin{bmatrix} y_1 \\ y_2 \end{bmatrix} = \begin{bmatrix} 1 + e_{12} & 0 \\ -e_{11} & 1 \end{bmatrix} \begin{bmatrix} u_1 \\ u_2 \end{bmatrix} \tag{12}$$

to yield the system in a more convenient form

$$\dot{u}_1 = u_2 + f_{u1} + \text{h.o.t.}, \quad \dot{u}_2 = \mu_1 u_1 + \mu_2 u_2 + f_{u2} + \text{h.o.t.}, \tag{13}$$

where h.o.t. are of orders $O(|y_i^5|)$, $O(|\varepsilon_i y_i^3|)$ and $O(|\varepsilon_i^2 y_i|)$, and the relevant symbols are defined in Appendix A.

At this stage, the method of normal forms is employed to simplify the reduced system in which the qualitative dynamics are still reserved in the neighborhood of the origin. The basic idea of normal forms is to use a near-identity co-ordinate transformation in which all non-essential non-linear terms are eliminated. Thus, the truncated normal form is given by

$$\dot{z}_1 = z_2, \quad \dot{z}_2 = \mu_1 z_1 + \mu_2 z_2 + a z_1^3 + b z_1^2 z_2, \tag{14}$$

where $a = H(1 - a_{13}a_{31})/\Delta$, $b = -3Ha_{12}a_{13}a_{31}/\Delta$.

We directly deduce the dynamical behavior of the full system (10) on the center manifold near the critical degenerate system. The rescaling technique can be used to reduce the number of cases. Letting $z_1 \to r_1 z_1$, $z_2 \to r_2 z_2$, and $t \to r_3 t$, we obtained the following form:

$$\dot{z}_1 = z_2, \quad \dot{z}_2 = \mu_1' z_1 + \mu_2' z_2 + c z_1^3 - z_1^2 z_2, \tag{15}$$

where $\mu_1' = \mu_1 r_3^2$, $\mu_2' = \mu_2 r_3$, $r_1 = (a/c)^{1/2}/b$, $r_2 = -(a/c)^{3/2}/b^2$, $r_3 = -(bc/a)$, and $c = +1$ for $a > 0$, $c = -1$ for $a < 0$. There are two distinct cases ($c = \pm 1$) to be considered. By local bifurcation analysis, system (15) has been studied quit extensively (see Appendix B). We can consequently employ the unfolding results of Refs. [10,11] directly to give the dynamical behavior of the full system (5) on the center manifold near the critical degenerate.

3.2. The stability of the non-autonomous system

For the case when $\omega_X(t)$ and $\omega_Z(t)$ are time-varying function, the system is the non-autonomous system and the motion of system (4) can be solved analytically, approximately or numerically as $x = \theta_0(t)$, $y = \dot{\theta}_0(t)$, $z = I_0(t)$, which satisfies the following equation:

$$\ddot{\theta}_0 + D_1\dot{\theta}_0 + D_3\omega_Z \sin\theta_0 - 1/2 D_4\omega_Z^2 \sin 2\theta_0 + \dot{\omega}_X = D_2 I_0, \tag{16a}$$

$$\dot{I}_0 + D_5 I_0 = -D_6\theta_0 - D_7\dot{\theta}_0. \tag{16b}$$

Let the disturbed motion be $x = \theta_0(t) + x_1,\ y = \dot{\theta}_0(t) + x_2, z = I_0(t) + x_3$, where x_1, x_2, x_3 are deviations from their respective nominal conditions. The differential equation (4) for the disturbances is

$$\begin{aligned}\dot{x}_1 &= x_2,\\ \dot{x}_2 &= -D_1 x_2 + D_2 x_3 - D_{3t}\omega_Z(t)x_1 + D_{4t}\omega_Z^2(t)x_1 + O(x_1^2),\\ \dot{x}_3 &= -D_5 x_3 - D_6 x_1 - D_7 x_2,\end{aligned} \tag{17}$$

where $D_{3t} = D_3\cos(\theta_0(t))$, $D_{4t} = D_4\cos(2\theta_0(t))$, and $O(x_1^2)$ represents higher order terms.

The stability of the motion of the above system (17) is investigated by the Liapunov direct method. Now we take the Liapunov function of quadratic forms:

$$V(\lambda_1, \lambda_2) = \lambda_1 x_1^2/2 + \lambda_2 x_1 x_2 + x_2^2/2 + \lambda_2 D_2 x_3^2/(2D_6), \tag{18}$$

where λ_1 and λ_2 are undetermined positive constants. There exists a number of Liapunov function candidates varied with the proper value of λ_1, λ_2, in which each of Liapunov candidates can give the conditions sufficient for stability. By choosing a number of λ_1, λ_2 properly, we can obtain the conditions sufficient for asymptotical stability of motion of the feedback control system. We have the negative time derivative of V through Eq. (17) as

$$\begin{aligned}-\dot{V}(\lambda_1, \lambda_2) = {}& \lambda_2[D_{3t}\omega_Z(t) - D_{4t}\omega_Z^2(t)]x_1^2 + [\lambda_2 D_1 + D_{3t}\omega_Z(t) - \lambda_1 - D_{4t}\omega_Z^2(t)]x_1 x_2\\ &+ (D_1 - \lambda_2)x_2^2 + (\lambda_2 D_8 - D_2)x_2 x_3 + \lambda_2 D_9 x_3^2 + W_1^*,\end{aligned} \tag{19}$$

where $D_8 = D_2 D_7/D_6$, $D_9 = D_2 D_5/D_6$, and W_1^* represents higher order terms.

Since $-\dot{V}$ contains time explicitly, we must find a function W that does not contain time explicitly such that $-\dot{V} \geqslant W$. We take W as

$$\begin{aligned}W = {}& \lambda_2(D_2 + \lambda_3)x_1^2 + (\lambda_2 D_1 + D_2 - \lambda_1 + \lambda_3)x_1 x_2 + \lambda_2 x_2^2\\ &+ (\lambda_2 D_8 - D_2)x_2 x_3 + \lambda_4 x_3^2,\end{aligned} \tag{20}$$

where λ_3 and λ_4 are undetermined positive constants. By Sylvester's theorem [14], W is positive definite if

$$\lambda_2 > 0, \tag{21a}$$

$$\lambda_3 > -D_2 = -K_T/(A + A_g), \tag{21b}$$

$$\begin{aligned}&(D_1\lambda_2 + D_2 + \lambda_3) - \sqrt{\lambda_2(D_2 + \lambda_3)[4\lambda_2\lambda_4 - (D_8\lambda_2 - D_2)^2]/\lambda_4}\\ &< \lambda_1 < (D_1\lambda_2 + D_2 + \lambda_3) + \sqrt{\lambda_2(D_2 + \lambda_3)[4\lambda_2\lambda_4 - (D_8\lambda_2 - D_2)^2]/\lambda_4},\end{aligned} \tag{21c}$$

$$\lambda_4 > (D_2 - \lambda_2 D_8)^2/(4\lambda_2) > 0 \tag{21d}$$

are satisfied. Furthermore,

$$\begin{aligned}-\dot{V} - W = {}& \lambda_2[-D_2 + (D_{3t}\omega_Z - \lambda_3) - D_{4t}\omega_Z^2]x_1^2 + [-D_2 + (D_{3t}\omega_Z - \lambda_3)\\ &- D_{4t}\omega_Z^2]x_1 x_2 + (D_1 - 2\lambda_2)x_2^2 + (D_9\lambda_2 - \lambda_4)x_3^2 + W^*,\end{aligned} \tag{22}$$

where W^* represents the terms of higher degree. If the following inequalities are held, then $-\dot{V} - W \geqslant 0$ ($= 0$ only when $x_1 = 0,\ x_2 = 0,\ x_3 = 0$), i.e., $-\dot{V} - W$ is positive definite. So $-\dot{V}$ is

positive definite:

$$D_{4t} > 0, \quad \text{i.e., } -\pi/4 < \theta_0 < \pi/4,$$

$$\left(D_{3t} - \sqrt{D_{3t}^2 - 4D_{4t}(D_2 + \lambda_3)}\right)/(2D_{4t}) < \omega_Z < \left(D_{3t} + \sqrt{D_{3t}^2 - 4D_{4t}(D_2 + \lambda_3)}\right)/(2D_{4t}), \tag{23a}$$

$$\lambda_3 < D_{3t}^2/(4D_{4t}) - D_2, \tag{23b}$$

$$D_1 > 2\lambda_2 > 0, \tag{23c}$$

$$4\lambda_2(D_1 - 2\lambda_2) - [-D_2 + (D_{3t}\omega_Z - \lambda_3) - D_{4t}\omega_Z^2] > 0, \tag{23d}$$

i.e., if $\lambda_3 < D_{3t}^2/4D_{4t} - D_2 - 4\lambda_2(D_1 - 2\lambda_2)$, then

$$\omega_Z < \left(D_{3t} + \sqrt{D_{3t}^2 - 4D_{4t}[(D_2 + \lambda_3) + 4\lambda_2(D_1 - 2\lambda_2)]}\right)/(2D_{4t})$$

or

$$\omega_Z > \left(D_{3t} + \sqrt{D_{3t}^2 - 4D_{4t}[(D_2 + \lambda_3) + 4\lambda_2(D_1 - 2\lambda_2)]}\right)/(2D_{4t}). \tag{23e}$$

If $\lambda_3 > D_{3t}^2/(4D_{4t}) - D_2 - 4\lambda_2(D_1 - 2\lambda_2)$, then

$$\omega_Z \in \Re, \ \Re\text{: } \textit{real number}, \tag{23f}$$

$$\lambda_4 < D_9\lambda_2. \tag{23g}$$

By Sylvester's theorem, the sufficient condition for the positive definiteness of V is

$$\lambda_1 > \lambda_2^2 > 0. \tag{24}$$

From Eqs. (21c), (21d) and (24), we have

$$\lambda_L < \lambda_1 < \lambda_H,$$

where

$$\lambda_L = \left(\lambda_2^2, D_1\lambda_2 + D_2 + \lambda_3 - \sqrt{\lambda_2(D_2 + \lambda_3)[4\lambda_2\lambda_4 - (D_8\lambda_2 - D_2)^2]/\lambda_4}\right)_{max}, \tag{25a}$$

$$\lambda_H = D_1\lambda_2 + D_2 + \lambda_3 + \sqrt{\lambda_2(D_2 + \lambda_3)[4\lambda_2\lambda_4 - (D_8\lambda_2 - D_2)^2]/\lambda_4}. \tag{25b}$$

From Eqs. (21b) and (23c), we have

$$\lambda_H > 2\lambda_2^2 + D_2 + \lambda_3 + \sqrt{\lambda_2(D_2 + \lambda_3)[4\lambda_2\lambda_4 - (D_8\lambda_2 - D_2)^2]/\lambda_4} > \lambda_2^2. \tag{26}$$

So the parameter λ_1 can be chosen from the domain constrained by the above inequalities. Similarly by the former inequalities (21b), (23b), (23e) and (23f), we know that λ_3 can be chosen if

$$-D_2 < \lambda_3 < D_{3t}^2/4D_{4t} - D_2 \tag{27}$$

is held. From Eqs. (21d) and (23g), the parameter λ_4 also can be chosen as

$$(D_2 - D_8\lambda_2)^2/(4\lambda_2) < \lambda_4 < D_9\lambda_2, \tag{28}$$

i.e., the following inequalities are held:

$$\lambda_2 > D_2/D_8 \quad \text{for } D_8 \leqslant 2\sqrt{D_9}, \tag{29a}$$

$$D_2/(2\sqrt{D_9} + D_8) < \lambda_2 < D_2/(D_8 - 2\sqrt{D_9}) \qquad \text{for } D_8 > 2\sqrt{D_9}. \tag{29b}$$

From Eqs. (23a), (23c), (23e), and (23f) by properly selecting a suitable λ_2 of Eq. (29), and a number of λ_3 of Eq. (27), we can get the following conditions that assure both $V(\lambda_1, \lambda_2)$ and $-\dot{V}(\lambda_1, \lambda_2)$ are positive definite:

$$\begin{aligned} \omega_{Z1} &= 0 < \omega_Z < \omega_{Z2} = D_{3t}/D_{4t} \\ &= (D_3/D_4)(\cos(\theta_0)/\cos(2\theta_0))(\geqslant D_3/D_4) \quad \text{for } -\pi/4 < \theta_0 < \pi/4, \end{aligned} \tag{30a}$$

and

$$\begin{aligned} &D_1 > 2D_2/D_8 \quad \text{for } D_8 \leqslant 2\sqrt{D_9}, \\ &D_1 > 2D_2/(2\sqrt{D_9} + D_8) \quad \text{for } D_8 > 2\sqrt{D_9}. \end{aligned} \tag{30b}$$

According to the Liapunov asymptotical theorem, Eq. (30) is the condition sufficient for stability of the system, and the motion $(\theta, \dot{\theta}, I) = (\theta_0, \dot{\theta}_0, I_0)$ is asymptotically stable.

The conditions sufficient for instability of motion of the feedback control system are considered by using the Liapunov instability theorem. We construct the Liapunov function as

$$V(m_1, m_2) = -m_1 x_1^2/2 - m_2 x_1 x_2 + x_2^2/2 + m_2 D_2 x_3^2/(2D_6), \tag{31}$$

where m_1 and m_2 are undetermined positive constants. Then we have

$$\begin{aligned} -\dot{V}(m_1, m_2) = &- m_2[D_{3t}\omega_Z(t) - D_{4t}\omega_Z^2(t)]x_1^2 \\ &+ [-m_2 D_1 + D_{3t}\omega_Z(t) + m_1 - D_{4t}\omega_Z^2(t)]x_1 x_2 + 2m_2 D_2 x_1 x_3 \\ &+ (D_1 + m_2)x_2^2 + (m_2 D_8 - D_2)x_2 x_3 + m_2 D_9 x_3^2 + W_2^*, \end{aligned} \tag{32}$$

where W_2^* represents the terms of higher degree.

Since $-\dot{V}$ contains time explicitly, we must find a function W that does not contain time explicitly such that $-\dot{V} \geqslant W$. We take W as

$$\begin{aligned} W = &- m_2 e^- x_1^2 + (e^- - m_2 D_1 + m_1)x_1 x_2 + m_2 x_2^2 + 2m_2 D_2 x_1 x_3 \\ &+ (m_2 D_8 - D_2)x_2 x_3 + m_3 x_3^2, \end{aligned} \tag{33}$$

where $0 > e^- > -\infty$. By Sylvester's theorem, we know that W is positive definite if

$$\begin{aligned} &m_L < m_1 < m_H, \quad \text{where } m_L = D_1 m_2 - e^- - 2m_2\sqrt{-e^-}, \\ &\qquad\qquad\qquad\qquad m_H = D_1 m_2 - e^- + 2m_2\sqrt{-e^-}, \\ &m_{av} - m_D < m_1 < m_{av} + m_D, \quad \text{where} \end{aligned} \tag{34a}$$

$$m_{av} = D_1 m_2 - e^- + D_2 m_2 (D_8 m_2 - D_2)/m_3,$$
$$m_D = \sqrt{m_2 (D_2^2 m_2 + e^- m_3)[(D_8 m_2 - D_2)^2 - 4 m_2 m_3]/m_3^2}, \tag{34b}$$

$$m_2 > 0, \tag{34c}$$

$$0 < m_3 < (D_8 m_2 - D_2)^2/(4 m_2) \quad \text{for } 0 > e^- > -m_2 D_2^2/m_3, \tag{34d}$$

$$m_3 > (D_8 m_2 - D_2)^2/(4 m_2) \quad \text{for } e^- < -m_2 D_2^2/m_3 \tag{34e}$$

are satisfied. Furthermore,

$$-\dot{V} - W = m_2 (e^- - D_{3t}\omega_Z + D_{4t}\omega_Z^2) x_1^2 + (-e^- - D_{3t}\omega_Z - D_{4t}\omega_Z^2) x_1 x_2 + D_1 x_2^2 + (m_2 D_9 - m_3) x_3^2. \tag{35}$$

If the following inequalities hold, then $-\dot{V} - W \geqslant 0$, i.e., $-\dot{V}$ is positive definite:

$$D_{4t} > 0, \quad \text{i.e., } -\pi/4 < \theta_0 < \pi/4,$$

$$\omega_Z < (D_{3t} - \sqrt{D_{3t}^2 - 4 D_{4t} e^-})/(2 D_{4t}) \quad \text{or}$$
$$\omega_Z > (D_{3t} + \sqrt{D_{3t}^2 - 4 D_{4t} e^-})/(2 D_{4t}), \tag{36a}$$

$$D_1 > 0, \tag{36b}$$

$$(D_{3t} - \sqrt{D_{3t}^2 - 4 D_{4t} e^- + 16 D_1 D_{4t} m_2})/(2 D_{4t}) < \omega_Z < (D_{3t} + \sqrt{D_{3t}^2 - 4 D_{4t} e^- + 16 D_1 D_{4t} m_2})/(2 D_{4t}), \tag{36c}$$

$$m_3 < m_2 D_9. \tag{36d}$$

From Eqs. (34a), and (34b), if $m_L < m_{av} < m_H$ are satisfied, i.e., $(0, (D_2^2 - 2\sqrt{-e^-})/(D_2 D_8))_{max} < m_2 < (D_2^2 + 2\sqrt{-e^-})/(D_2 D_8)$, the parameter m_1 can be chosen. Similarly by the former inequalities (34d), (34e) and (36d), we know that m_3 can be selected. Also from equations (36a)–(36c), by properly selecting a number of e^-, we can get the conditions that assure $-\dot{V}(m_1, m_2)$ be positive definite:

$$\omega_Z < 0 \quad \text{or} \quad \omega_Z > D_{3t}/D_{4t}, \tag{37a}$$

$$D_1 > 0. \tag{37b}$$

According to the Liapunov instability theorem, Eqs. (37a) and (37b) are the condition sufficient for the unstable system. From the previous result, we can obtain conditions for sufficient of stability and instability of the motion $(\theta, \dot{\theta}, I) = (\theta_0, \dot{\theta}_0, I_0)$.

4. Singular perturbation model

To facilitate the analysis, in the interest of model simplification, we usually neglect those small physical parameters to reduce orders of a model. Singular perturbations are used to simplify the model and to provide tools for improving oversimplified models when the original full order model satisfies the some assumptions [12]. To obtain the standard singular perturbation model, let us define the variables $p_1 = x$, $p_2 = T_m y$, $q = (T_m^2 D_2)z$, $t \to t/T_m$, $T_m = D_5/(D_1 D_5 + D_2 D_7)$, $T_e = 1/D_5$, $\varepsilon = T_e/T_m$, and rewrite the state equation (4) as

$$\begin{aligned} \dot{p}_1 &= p_2, \\ \dot{p}_2 &= -a_0 p_2 + q - a_3 \omega_Z(t) \sin p_1 + 1/2 a_4 \omega_Z^2(t) \sin 2p_1 - \dot{\omega}_X(t), \\ \varepsilon \dot{q} &= -q - a_1 p_1 - a_2 p_2, \end{aligned} \tag{38}$$

or in the compact form $\dot{p} = f_0(t, p, q, \varepsilon)$, $\varepsilon \dot{q} = g_0(t, p, q, \varepsilon)$, where $p = [p_1,\ p_2]$, $f_0 = [f_{01}, f_{02}]$, $a_0 = D_1 T_m$, $a_1 = D_2 D_6 T_m^2/D_5$, $a_2 = D_2 D_7 T_m/D_5$, $a_3 = D_3 T_m^2$, $a_4 = D_4 T_m^2$.

We assume that $\varepsilon \ll 1$. This assumption means that the mechanical time constant T_m is sufficiently larger than the electrical time constant T_e. By using the singular perturbation theory [13] to consider the singularly perturbed system (38), at $\varepsilon = 0$, the slow manifold is

$$q = h(t, p) = -a_1 p_1 - a_2 p_2.$$

The corresponding slow model, $\dot{p} = f_0(t, p, h(t, p), 0)$,

$$\dot{p}_1 = p_2, \quad \dot{p}_2 = -M(p_1, \omega_Z) - N(p_2) - \dot{\omega}_X, \tag{39}$$

where $M(p_1, \omega_Z) = a_1 p_1 + a_3 \omega_Z(t) \sin p_1 - a_4 \omega_Z^2(t) \cos p_1 \sin p_1$, $N(p_2) = (a_0 + a_2) p_2$.

For the case when $\dot{\omega}_X = 0$ and $\omega_Z = \omega_{ZC} = const.$, the system has one isolated equilibrium point at the origin. Depending upon the functions $M(\cdot)$ and $N(\cdot)$ it might have other equilibrium points. A Lyapunov function candidate may be taken as the energy-like function

$$V(p) = \int_0^{p1} M(y, \omega_{ZC})\, \mathrm{d}y + 1/2 p_2^2. \tag{40}$$

The derivative of $V(p)$ along the trajectories of the system is given by

$$\dot{V}(p) = -p_2 N(p_2) \leqslant 0. \tag{41}$$

Thus, $\dot{V}(p)$ is negative semidefinite. According to the theorems of Barbashin and Krasovskii [13], the only solution of the system that can stay in $S = \{p \in \Re^2 \mid p_2 = 0\}$ for all t is the trivial solution $p(t) = 0$ if $M(0, \omega_{ZC}) = 0$, $p_1 M(p_1, \omega_{ZC}) > 0$ for $p_1 \neq 0$ is satisfied , i.e.,

$$\begin{aligned} &p_1(a_1 p_1 + a_3 \omega_{ZC} \sin p_1 - a_4 \omega_{ZC}^2 \cos p_1 \sin p_1) \\ &\quad > p_1(a_1 \sin p_1 + a_3 \omega_{ZC} \sin p_1 - a_4 \omega_{ZC}^2 \sin p_1) > 0 \end{aligned} \tag{42}$$

when the condition

$$(a_3 - \sqrt{a_3^2 + 4 a_1 a_4})/(2a_4) < \omega_{ZC} < (a_3 + \sqrt{a_3^2 + 4 a_1 a_4})/(2a_4) \tag{43}$$

is held. Thus, the origin is asymptotically stable.

For the case when $\dot{\omega}_X(t)$ and $\omega_Z(t)$ are time-varying function, the system has an exponentially stable motion $(p_1, \dot{p}_1) = (p_{10}(t), \dot{p}_{10}(t))$ when the following condition is held:

$$\omega_{Z1} < \omega_Z(t) < \omega_{Z2}, \tag{44}$$

where

$$\omega_{Z1} = (a_{3t} - \sqrt{a_{3t}^2 + 4a_1 a_{4t}})/(2a_{4t}) = (D_{3t} - \sqrt{D_{3t}^2 + 4D_2 D_{4t}(D_6/D_5)})/(2D_{4t}),$$

$$\omega_{Z2} = (a_{3t} + \sqrt{a_{3t}^2 + 4a_1 a_{4t}})/(2a_{4t}) = (D_{3t} + \sqrt{D_{3t}^2 + 4D_2 D_{4t}(D_6/D_5)})/(2D_{4t})$$

and $D_{4t} > 0$, i.e., $-\pi/4 < \theta_0 < \pi/4$, $a_{3t} = a_3 \cos(p_{10})$, $a_{4t} = a_4 \cos(2p_{10})$ which can be derived by the same form of Liapunov functions as Ref. [4]. The origin of the corresponding boundary-layer system

$$\frac{\mathrm{d}\gamma}{\mathrm{d}\tau} = g_0(t, p, \gamma + h(t, p), 0) = -\gamma \tag{45}$$

is exponentially stable uniformly in (t, p). Since f_0 and g_0 of Eq. (38) also satisfy the conditions of Appendix C, we conclude that the origin of the full singularly perturbed system (38) is exponentially stable for sufficiently small ε. Thus, the necessary and sufficient condition for asymptotic stability is Eq. (44).

From Sections 3 and 4 analyses, condition (30) sufficient for asymptotical stability of Section 3 are covered by Eq. (44) of Section 4, i.e.,

$$\omega_{Z1} < \left\{ \begin{array}{ll} 0 < \omega_Z(t) < D_{3t}/D_{4t} & \text{Eq.(30)} \\ \omega_Z(t) & \text{Eq.(44)} \end{array} \right\} < \omega_{Z2}.$$

The result of Section 4 has larger stability region than that of Section 3. In Section 3, a three-dimensional dynamic system is considered. In Section 4, we consider the case in which the mechanical time constant is sufficiently larger than the electrical time constant. Thus the system can be reduced to a two-dimensional system by singular perturbations which simply the order of the model and provide tools for improving oversimplified models.

5. Numerical demonstrations

In this section, examples are carried out to examine the various forms of dynamic behavior of system (4) for the previous analyses by numerical simulation techniques. The parameters of the cases are shown in Appendix D.

In Section 3.1, the stability condition (7) for the non-linear autonomous system is derived and the numerical simulations of the autonomous system (5) near the double-zero degenerate point are analyzed. The double-zero eigenvalues with the third eigenvalue $\lambda_3 = -165$ of the system and the stability boundary of the uncertain constant angular velocity ω_{ZC} are obtained corresponding to the double-zero degenerate point $(D_{2C}, Q_C) = (388.889, 3888.89)$. There exists at least one zero eigenvalue of the system at $Q = e_6$, the maximum eigenvalue that is equal to zero is presented by the solid line and the stability boundary of the uncertain constant angular velocity ω_{ZC} corresponding to $Q = e_6$ are obtained as shown in Fig. 2. A pair of pure imaginary eigenvalues exist corresponding to the solid line of $Q = e_3$ and the stability boundary of the uncertain constant

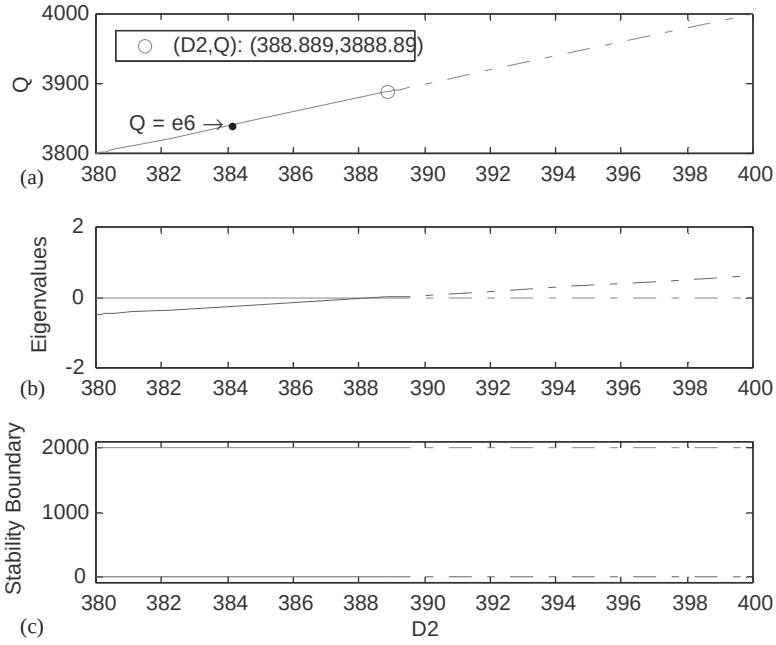

Fig. 2. Stability analysis of the autonomous system (5) near the double-zero degenerate point $(D_{2C}, Q_C) = (388.889, 3888.89)$: (a) one zero eigenvalue at $Q = e_6$; (b) two maximum eigenvalues of the system corresponding $Q = e_6$; (c) the stability boundary of the uncertain constant angular velocity ω_{ZC} corresponding $Q = e_6$.

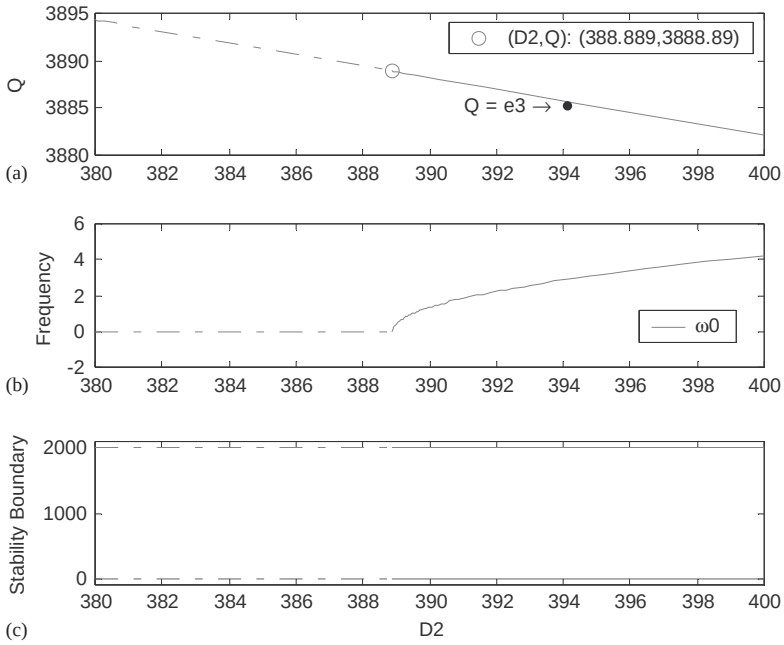

Fig. 3. Stability analysis of the autonomous system (5) near the double-zero degenerate point $(D_{2C},\ Q_C) = (388.889, 3888.89)$: (a) one eigenvalue with zero real part at $Q = e_3$; (b) a pair of pure imaginary eigenvalues corresponding $Q = e_3$; (c) the stability boundary of the uncertain constant angular velocity ω_{ZC} corresponding $Q = e_3$.

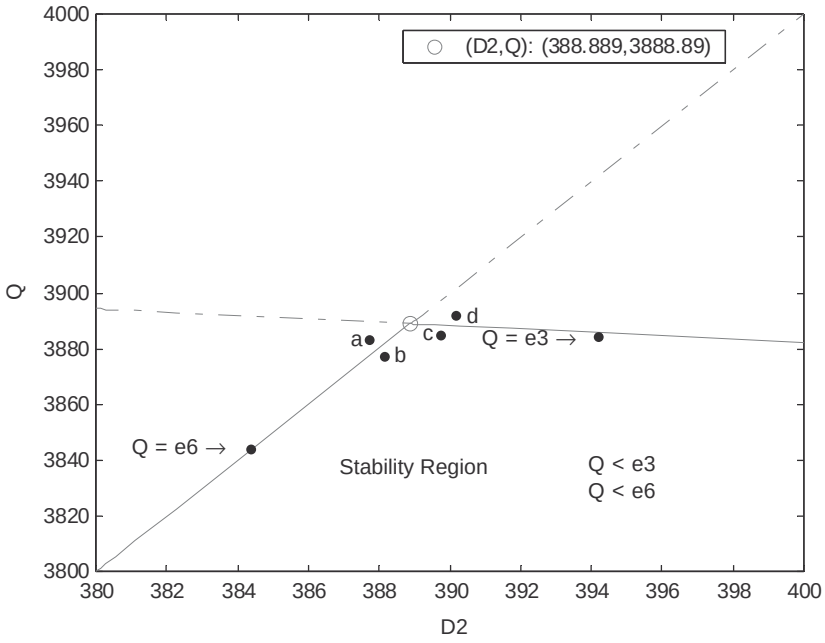

Fig. 4. Stability region of the autonomous system (5) near the double-zero degenerate point $(D_{2C}, Q_C) = (388.889, 3888.89)$.

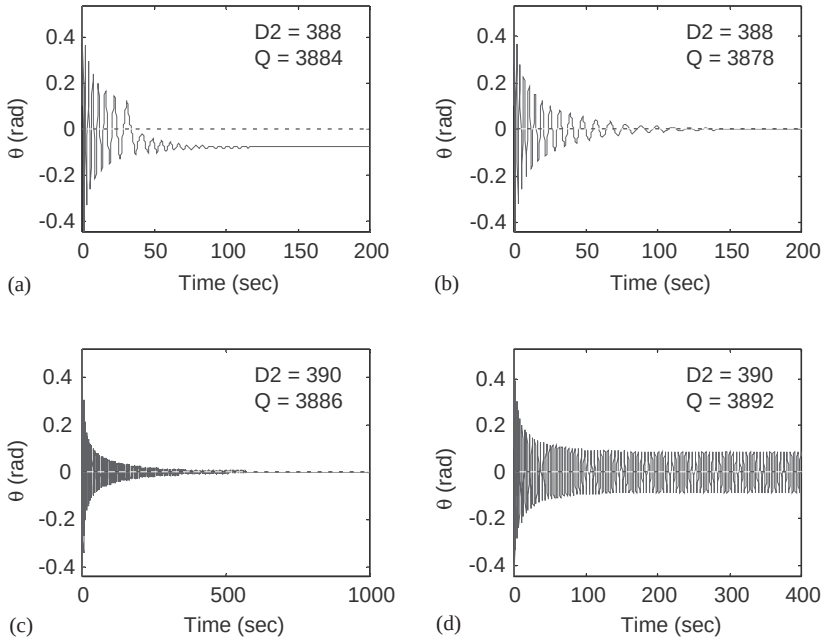

Fig. 5. The time histories of the autonomous system (5) near the double-zero degenerate point $(D_2, Q) = (388.889, 3888.89)$: (a) 'a' point $(D_2, Q) = (388, 3884)$; (b) 'b' point $(D_2, Q) = (388, 3878)$; (c) 'c' point $(D_2, Q) = (390, 3886)$; (d) 'd' point $(D_2, Q) = (390, 3892)$.

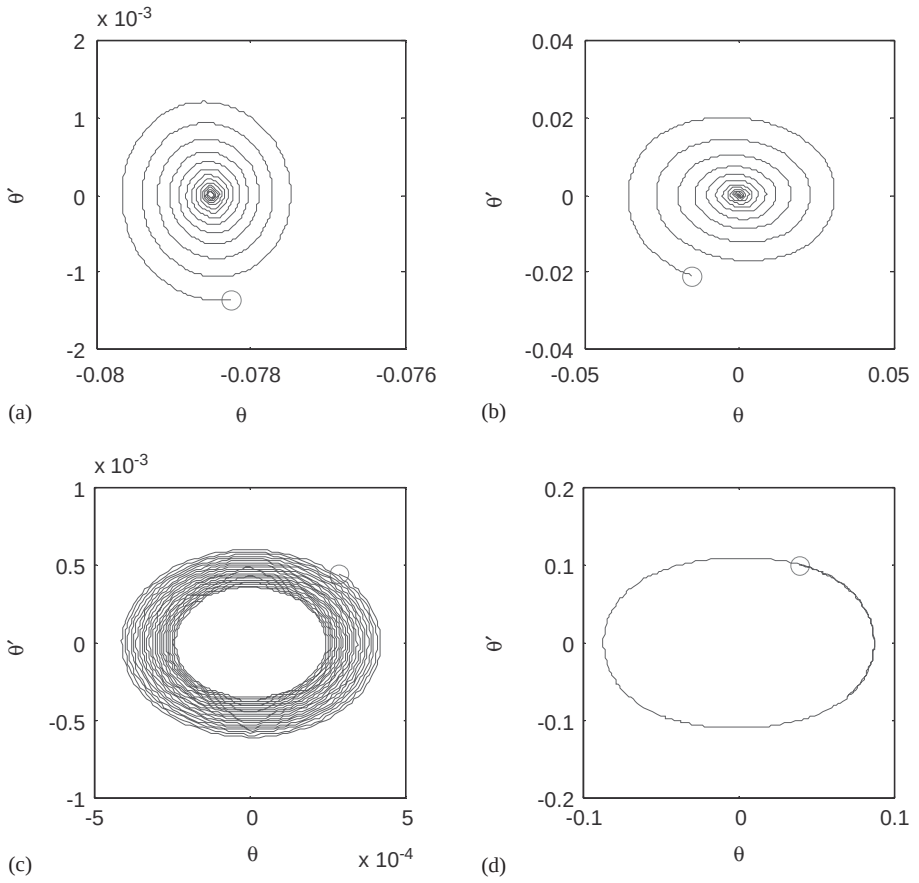

Fig. 6. The phase trajectories of the autonomous system (5) near the double-zero degenerate point $(D_2, Q) = (388.889, 3888.89)$: (a) 'a' point $(D_2, Q) = (388, 3884)$; (b) 'b' point $(D_2, Q) = (388, 3878)$; (c) 'c' point $(D_2, Q) = (390, 3886)$; (d) 'd' point $(D_2, Q) = (390, 3892)$ in Fig. 5.

angular velocity ω_{ZC} corresponding to $Q = e_3$ are obtained in Fig. 3. Stability regions of the autonomous system (5) near the double-zero degenerate point are obtained as shown in Fig. 4 when both the inequality conditions $Q < e_6$ and $Q < e_3$ are satisfied. The time-historical trajectories of the perturbed motion that converge to the origin from the initial state $(x_1, x_2, x_3) = (0.1, 0, 0)$ are plotted in Figs. 5(b) and (c) for 'b' and 'c' points are within stability region in Fig. 4. These systems are locally asymptotical stable. On the other hand, Figs. 5(a) and (d) show that the trajectories move far away from the origin to another fixed point and limit cycle, respectively, for 'a' and 'd' points are beyond stability region in Fig. 4. This means that the systems are unstable. Similarly, the phase trajectories corresponding Fig. 5 are presented as shown in Fig. 6. Also, the dynamics of the autonomous system (5) on the center manifold near the double-zero degenerate point are examined. In Fig. 7, we illustrate a bifurcation set in (D_2, Q) space for Eq. (15), $c = -1$, with the associated phase portraits which are topologically equivalent to the flow on the center manifold.

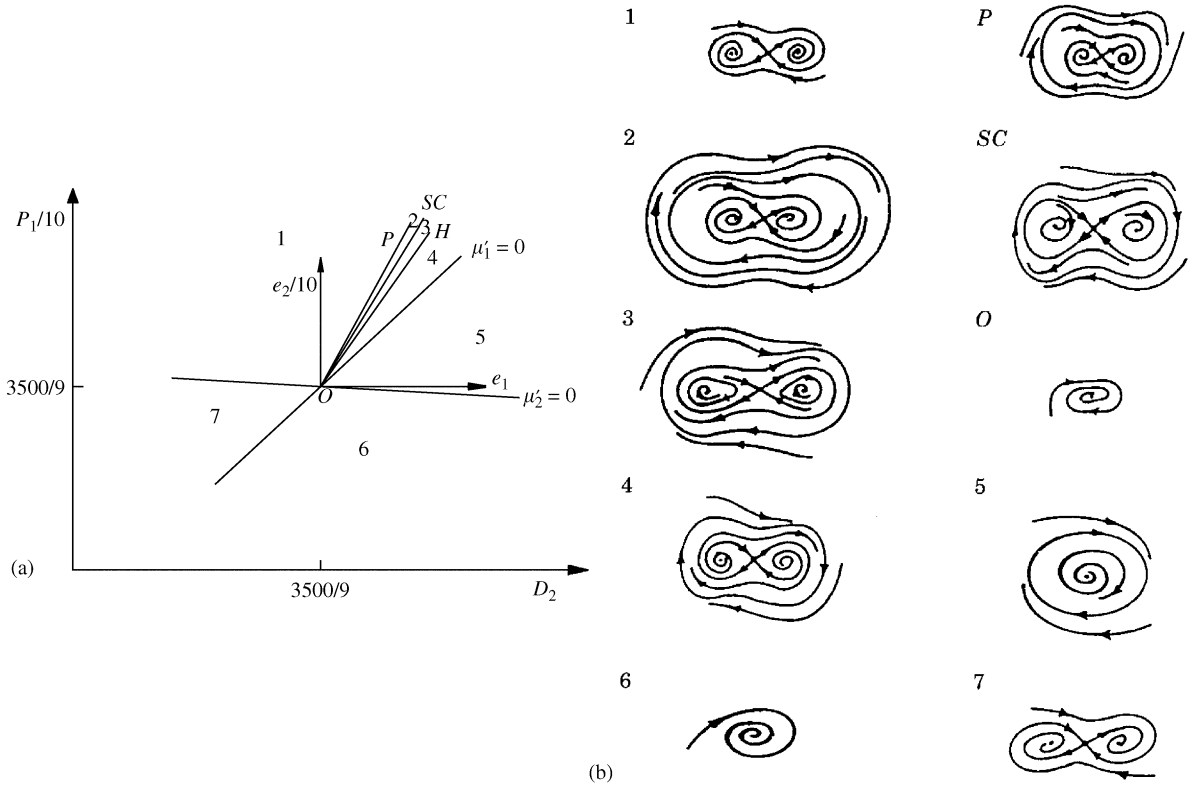

Fig. 7. Bifurcation diagram near the degenerate point (D_{2C}, Q_C): (a) bifurcation set in (D_2, Q) space; (b) the associated phase portraits; H: Hopf bifurcation, SC: saddle connection bifurcation, P: saddle-node bifurcation of cycles, $\mu_1' = 0$: pitchfork bifurcation.

From stability analyses of the non-autonomous system, in Sections 3.2 and 4, the sufficient condition (30) for stability are covered by condition (44) and the latter must satisfy the condition when the mechanical time constant is sufficiently larger than the electrical time constant. Then those are very close. When the parameters of the gyro satisfy the stability condition, i.e., $\omega_{Z1} < \omega_Z < \omega_{Z2}$, the motion is asymptotically stable.

For the case $\dot{\omega}_X(t)$ is time-varying function but small, the solution of the dynamic system can be assumed zero. In the parameters $D_1 = 1$, $D_2 = 10$, we have the limits $\omega_{Z1} = 0$, $\omega_{Z2} = 2000$ for the stability condition (30), and the limits $\omega_{Z1} = -0.05$, $\omega_{Z2} = 2000.05$ for the stability condition (44). When $\omega_Z(t)$ varies between ω_{Z1} and ω_{Z2} the gimbals motion is asymptotically stable. The case $\omega_Z(t) = \omega_{ZC} + v \sin \omega t$ oscillating near the stability boundary ω_{Z2} is studied by numerical simulation of system (4) as shown in Figs. 8 and 9. In Figs. 8(a) and (b), the trajectories of the perturbed motion asymptotically converges to the origin from the initial state $(x_1,\ x_2,\ x_3) = (0.1, 0, 0)$ when $\omega_Z(t)$ oscillates between ω_{Z1} and ω_{Z2}. The quasiperiodic trajectory is restricted to an annular-like region of the state space and the corresponding Poincaré map points fill in an elliptically shaped closed curve for $\omega_{ZC} = 2000, v = 0.415$ at the fixed driving frequency $\omega = 30$ in Fig. 8(c) and (d), respectively. A limit cycle of period-T plotted in phase plane

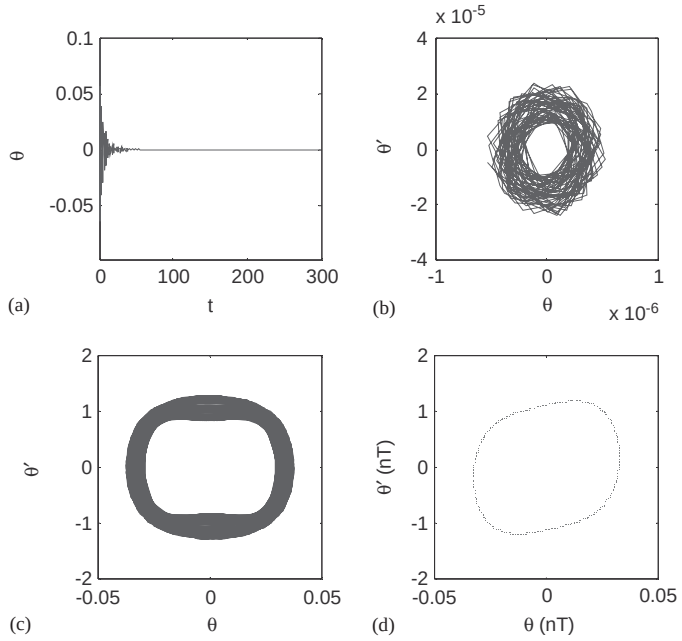

Fig. 8. The numerical simulation of the non-autonomous system (4): (a) the time history; (b) the phase trajectory for $\omega_Z(t) = 1999 + 0.415\sin(30t)$; (c) the phase trajectory; (d) Poincaré map for $\omega_Z(t) = 2000 + 0.415\sin(30t)$.

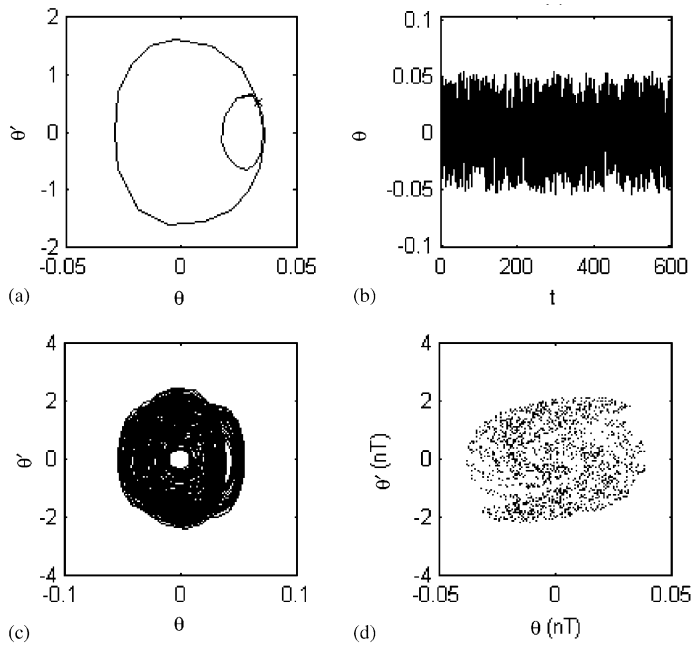

Fig. 9. The numerical simulation of the non-autonomous system (4): (a) the phase trajectory for $\omega_Z(t) = 2000 + 1.25\sin(30t)$; (b) the time history; (c) the phase trajectory; (d) Poincaré map for $\omega_Z(t) = 2000 + 1.31\sin(30t)$.

for $v = 1.25$ as shown in Fig. 9(a). From Figs. 9(b) and (d), the time history, phase portraits and Poincaré maps exhibit the chaotic motion of the system for $v = 1.31$.

6. Conclusions

An analysis is presented of a single-axis rate gyro subjected to linear feedback control when the vehicle is simultaneously spinning with uncertain angular velocity $\omega_Z(t)$ about its spin axis and accelerating $\dot{\omega}_X(t)$ with respect to the output axis of the gyro. For the autonomous case in which ω_Z is steady, both stability and degeneracy conditions of the fixed point were derived by the Routh–Hurwitz criterion in Section 3.1. The autonomous system reveals the existence of saddle connection, pitchfork, and Hopf bifurcations near the double degeneracy by local bifurcation analyses. A bifurcation set and the associated sequence of phase portraits on the center manifold are presented. For the non-autonomous case where $\omega_Z(t)$ and $\dot{\omega}_X(t)$ are time-varying, there are explicit functions of time, which were considered as coefficients, are contained by the differential equation of motion. It is more difficult to find the Liapunov function candidate than that of the autonomous system by using the Liapunov direct method. The conditions sufficient for asymptotic stability and instability of motion were obtained in Section 3.2. In Section 4, the electric time constant is much smaller than the mechanical time constant assumed. Then modelling this physical system in the singularly perturbed form can be found. The stability of a full singular perturbed system from the reduced and boundary-layer systems was studied in both autonomous and non-autonomous systems by the Liapunov direct method for sufficiently small ε. In this paper, the model considered here provides not only conditions sufficient for asymptotic stability for design but also the existence of periodic, quasiperiodic and chaotic motions of the system. Finally, the occurrence and nature of chaotic attractors were studied by evaluating the time history, phase plane and Poincaré maps.

Acknowledgements

The authors are grateful to the National Science Council, Republic of China, for supporting this research under Grant NSC 90-2218-E-164-001.

Appendix A

(a) $a_{12} = -(-D_6 + D_5D_7)/(D_5D_6)$, $a_{13} = D_1/D_6 - D_1(D_1 + D_5)D_7/(D_6(-D_6 + (D_1 + D_5)D_7))$,
$a_{23} = D_1(D_1 + D_5)/(-D_6 + (D_1 + D_5)D_7)$, $a_{31} = -D_6/D_5$, $\Delta = \det(\mathbf{T}) = 1 - a_{13}a_{31} + a_{12}a_{23}a_{31}$.

(b)
$$\Lambda = \begin{bmatrix} 0 & 1 & 0 \\ 0 & 0 & 0 \\ 0 & 0 & -D_1 - D_5 \end{bmatrix}, \quad \Lambda_\varepsilon = \begin{bmatrix} e_{11} & e_{12} & e_{13} \\ e_{21} & e_{22} & e_{23} \\ e_{31} & e_{32} & e_{33} \end{bmatrix}, \quad F_y = T^{-1}F(Ty) = \begin{bmatrix} f_{y1} \\ f_{y2} \\ f_{y3} \end{bmatrix},$$

$e_{11} = -a_{12}(a_{31}e_1 + e_2)/\Delta$, $e_{12} = -a_{12}^2e_2/\Delta$, $e_{13} = -a_{12}(e_1 + a_{13}e_2)/\Delta$,
$e_{21} = (1 - a_{13}a_{31})(a_{31}e_1 + e_2)/\Delta$, $e_{22} = a_{12}(1 - a_{13}a_{31})e_2/\Delta$, $e_{23} = (1 - a_{13}a_{31})(e_1 + a_{13}e_2)/\Delta$,

$e_{31} = a_{12}a_{31}(a_{31}e_1 + e_2)/\Delta$, $e_{32} = a_{12}^2 a_{31}e_2/\Delta$, $e_{33} = a_{12}a_{31}(e_1 + a_{13}e_2)/\Delta$, $f_{y1} = -a_{12}f_{y0}$, $f_{y2} = (1 - a_{13}a_{31})f_{y0}$, $f_{y3} = a_{12}a_{31}f_{y0}$, $f_{y0} = H(y_1 + a_{12}y_2 + a_{13}y_3)^3/\Delta$.

(c) $f_{yc1} = -a_{12}f_{yc0}$, $f_{yc2} = (1 - a_{13}a_{31})f_{yc0}$, $f_{yc0} = H(y_1 + a_{12}y_2)^3/\Delta$.

(d) $\mu_1 = e_{21} = [(1 - a_{13}a_{31})a_{31}/\Delta]e_1 + [(1 - a_{13}a_{31})/\Delta]e_2$, $\mu_2 = e_{11} + e_{22} = -(a_{12}a_{31}/\Delta)e_1 - (a_{12}a_{13}a_{31}/\Delta)e_2$, $f_{u1} = -a_{12}f_{u0}$, $f_{u2} = (1 - a_{13}a_{31})f_{u0}$, $f_{u0} = H(u_1 + a_{12}u_2)^3/\Delta$.

Appendix B

Here, only an outline of the basic information needed for our special purpose is given by Wiggins [16]. First, the system equilibrium points are determined as follows:

$$c = +1{:}(0,0), (\pm\sqrt{-\mu_1'}, 0), \quad c = -1{:}(0,0), (\pm\sqrt{\mu_1'}, 0).$$

By checking the linearized stability for these fixed points, the following bifurcation sets occur:

$c = +1$: pitchfork on $\mu_1' = 0$, supercritical Poincaré–Andronov–Hopf on $\mu_1' < 0$, $\mu_2' = 0$,

$c = -1$: pitchfork on $\mu_1' = 0$, subcritical Poincaré–Andronov–Hopf on $\mu_1' = \mu_2'$, $\mu_1' > 0$.

By using Bendixson's criterion and index theory, Eq. (15) has no periodic orbits for

$$c = +1{:}\ \mu_1' > 0; \quad \mu_1' < 0,\ \mu_2' < 0; \quad \mu_2' > -\mu_1'/5, \quad \mu_1' < 0, \quad c = -1{:}\ \mu_2' < 0.$$

The results above are shown in Fig. 7 for $c = -1$.

In addition the pitchfork and Hopf bifurcations for local analyses, a saddle-connection or homoclinic bifurcation for global analyses is considered below to complete the bifurcation diagram.

For $c = +1$, using the rescaling $z_1 = \varepsilon u$, $z_2 = \varepsilon^2 v_1$, $\mu_1' = -\varepsilon^2$, $\mu_2' = \varepsilon^2 v_2$ and $t \to \varepsilon t$, the rescaled form of system (15) is given by $\dot{u} = v_1$, $\dot{v}_1 = -u + u^3 + \varepsilon(v_2 v_1 - u^2 v_1)$. For $\varepsilon = 0$, the Hamiltonian function of this system is $H(u, v_1) = v_1^2/2 + u^2/2 - u^4/4$. The autonomous system has a heteroclinic connection on $\mu_2' = -\mu_1'/5 + O(\mu_1'^2)$.

For $c = -1$, using the rescaling $z_1 = \varepsilon u$, $z_2 = \varepsilon^2 v_1$, $\mu_1' = \varepsilon^2$, $\mu_2' = \varepsilon^2 v_2$ and $t \to \varepsilon t$, the rescaled form of system (15) is given by $\dot{u} = v_1$, $\dot{v}_1 = u - u^3 + \varepsilon(v_2 v_1 - u^2 v_1)$. For $\varepsilon = 0$, the Hamiltonian function of this system is $H(u, v_1) = v_1^2/2 - u^2/2 + u^4/4$. The autonomous system has a homoclinic bifurcation on $\mu_2' = 4\mu_1'/5 + O(\mu_1'^2)$ and a saddle-node bifurcation of cycles on $\mu_2' = d\mu_1' + \cdots$, $d \approx 0.752$, on which the periodic orbits coalesce.

Appendix C

The stability analysis that describes a procedure for constructing Liapunov functions for full singularly perturbed system as follows [13]:

Consider the singularly perturbed non-autonomous system

$$\dot{x} = f(t, x, z, \varepsilon), \quad \varepsilon\dot{z} = g(t, x, z, \varepsilon). \tag{C.1}$$

Assume that the following assumptions are satisfied for all $(t, x, \varepsilon) \in [0, \infty) \times B_r \times [0, \varepsilon_0]$:

1. $f(t, 0, 0, \varepsilon) = 0$ and $g(t, 0, 0, \varepsilon) = 0$.
2. The equation $0 = g(t, x, z, 0)$ has an isolated root $z = h(t, x)$ such that $h(t, x) = 0$.
3. The functions f, g and h and their partial derivatives up to order 2 are bounded for $z - h(t, x) \in B_\rho$.

4. The origin of the reduced system $\dot{x} = f(t, x, h(t, x), 0)$ is exponentially stable.
5. The origin of the boundary-layer system $dy/d\tau = g(t, x, y + h(t, x), 0)$ is exponentially uniformly stable in (t, x).

Then there exists $\varepsilon^* > 0$ such that, for all $\varepsilon < \varepsilon^*$, the origin of Eqs. (C.1) is exponentially stable.

Appendix D

The values of gyro parameters:

$$(A + A_g) = 54 \text{ dyne cm s}^2, \quad Cn_R = 10.8 \times 10^4 \text{dyne cm s}, \quad C_d = 7560 \text{ dyne cm rad}^{-1}\, s,$$

$$D_1 = \frac{C_d}{(A + A_g)} = 130 \sim 150 \text{ rad}^{-1}\text{s}^{-1}, \quad D_2 = \frac{K_T}{(A + A_g)} = 380 \sim 400 \text{ A}^{-1} \text{ rad}^{-2}\text{s}^{-2},$$

$$D_3 = \frac{Cn_R}{(A + A_g)} = 2000 \text{ s}^{-1}, \quad D_4 = \frac{(A + B_g - C_g)}{(A + A_g)} = 1, \quad D_5 = R/L = 25 \text{ s}^{-1},$$

$$D_6 = K_a/L = 250 \text{ A rad}^{-1}\text{ s}^{-1}, \quad D_7 = K_0/L = 1 \text{ A rad}^{-1}.$$

References

[1] S.N. Singh, Stability of gyro in a vehicle spinning with uncertain angular vehicle, *IEEE Transactions on Aerospace and Electronic Systems* AES-17 (1981) 208–211.
[2] S.N. Singh, Stability of gyro with harmonic nonlinearity in spinning vehicle, *IEEE Transactions on Aerospace and Electronic Systems* AES-19 (1983) 182–189.
[3] S.N. Singh, Gyro motion boundedness under uncertain vehicle spin and acceleration, *IEEE Transactions on Aerospace and Electronic Systems* AES-20 (1984) 119–127.
[4] Z.M. Ge, C.J. Chen, Stability of a rate gyro, *American Institute of Aeronautics and Astronautics Journal of Guidance, Control, and Dynamics* 15 (1992) 1034–1036.
[5] Z.M. Ge, H.H. Chen, Stability and chaotic dynamics of a rate gyro with feedback control, *Japanese Journal of Applied Physics* 36 (1997) 5373–5381.
[6] Z.M. Ge, H.H. Chen, Double degeneracy and chaos in a rate gyro with feedback control, *Journal of Sound and Vibration* 209 (5) (1998) 753–769.
[7] F.C. Moon, *Chaotic Vibrations*, Wiley, New York, 1987.
[8] J.M.T. Thompson, H.B. Stewart, *Nonlinear Dynamics Chaos*, Wiley, Chichester, 1986.
[9] M. Laskshmanan, K. Murali, *Chaos in Nonlinear Oscillators: Controlling and Synchronization*, World Scientific, Singapore, 1996.
[10] P. Holmes, Dynamics of a nonlinear oscillator with feedback control I: local analysis, *Journal of Dynamic System Measurement and Control* 107 (1985) 159–165.
[11] J. Guckenheimer, P. Holmes, *Nonlinear Oscillations, Dynamical Systems and Bifurcation of Vector Fields*, Springer, New York, 1986, Chapters 4–7.
[12] G. Peponides, P.V. Kokotovic, J.H. Chow, Singular perturbations and time scales in nonlinear models of power systems, *IEEE Transactions on Circuits and Systems* CAS-29 (1982) 758–767.
[13] H.K. Khalil, *Nonlinear Systems*, Macmillan, New York, 1992, Chapters 3,4,8.
[14] L. Meirovitch, *Method of Analytical Dynamics*, McGraw-Hill, New York, 1970, Chapters 6–10.
[15] J. Carr, *Applications of Centre Manifold Theory*, Springer, New York, 1981.
[16] S. Wiggins, *Global Bifurcations and Chaos*, Springer, New York, 1988.